Nonequilibrium Processes in Supersonic Jets of N_2, H_2, and $N_2 + H_2$ Mixtures: (II) Shock Waves

A. Ramos,*,† G. Tejeda, J. M. Fernández, and S. Montero

Laboratory of Molecular Fluid Dynamics, Instituto de Estructura de la Materia, CSIC, Serrano 121, 28006 Madrid, Spain

Received: May 3, 2010; Revised Manuscript Received: June 14, 2010

We report an experimental study of the shock wave system of three continuous axisymmetric jets of pure N_2 and H_2, and of the $N_2 + 2H_2$ mixture, generated at $p_0 = 1$ bar and $T_0 = 295$ K through a $D = 310$ μm cylindrical nozzle against a background pressure $p_b = 6.1$ mbar. Number density and rotational populations have been measured by Raman spectroscopy with high spatial resolution ($\sim$15 μm) across the normal shock wave located at $z/D \approx 8$, and across the barrel shock wave at the plane $z/D = 5.2$. Significant differences in position, widths, and gradients of the shock waves are observed among the three jets. Such differences are qualitatively interpreted in terms of disparity in mass, inelastic cross sections, and collision numbers. Non-Boltzmann distributions of the rotational populations of N_2 are observed within the shock waves at regions where the local Knudsen number is higher than 0.05. In the $N_2 + 2H_2$ mixture the different behavior of the two species leads to a localized enrichment of the light component up to 20%, which might provide the basis for an efficient separation device. Measurements on the invasion of the shock wave system by the background molecules are also reported, proving such invasion to be more efficient for the lighter species H_2 than for the heavier N_2.

Introduction

Gas shock waves are generated in different natural and artificial processes. In a supersonic free jet, a system of shock waves adjusts the jet to downstream boundary conditions, changing the flow line directions and reducing the velocity. For axisymmetric jets, such a system is formed by a normal shock wave (Mach disk) perpendicular to the jet axis, and by a barrel shock wave that encapsulates the zone of silence of the jet.[1] Shock waves are characterized by strong density, temperature, and velocity gradients, and also by a bimodal distribution of temperatures.[2,3] In addition, shock waves of molecular gases show a strong breakdown of equilibrium between translational and internal degrees of freedom.[4,5]

Several experimental techniques have been employed for studying shock waves in gas jets: electron-beam-induced fluorescence,[3,6,7] electron-beam absorption,[8] laser-induced fluorescence,[9] Rayleigh scattering,[10] and Raman spectroscopy.[11,12] Although most of these experiments have been devoted to measuring macroscopic quantities, some of them have studied at microscopic scale the evolution of velocity[3,9] and rotational distribution functions[7,11] across the normal shock wave. Theoretical interpretation of shock waves rests to date on the numerical solution of Boltzmann equation[4,5] and on gas-dynamics approaches.[12,13]

Most earlier works on shock waves have been constrained to single-species gases.[4,5,12,13] Shock waves in gas mixtures, however, pose a somewhat different problem, which has been investigated by Monte Carlo direct simulation[4,14,15] and by numerical solution of Boltzmann equation.[16,17] A major topic is the study of shock waves over blunt bodies and their associated relaxation phenomena.[15,18] Another problem, not yet fully understood, is the interaction of the background gas with the zone of silence of a supersonic jet through normal and barrel shock waves. This interaction, which leads to the preferential invasion of the lighter species, has been employed for separation of species and isotopes.[19,20] Experimental data on shock waves in mixtures are not abundant nor easy to obtain, mostly being constrained to He + Ar mixtures,[21–23] with even less results on molecular mixtures.[24]

In a previous work,[25] hereinafter referred to as paper I, we studied the zone of silence of supersonic jets of pure N_2 and H_2, and of the $N_2 + 2H_2$ and $2N_2 + H_2$ mixtures. Here, we widen this study with measurements on shock waves in jets of N_2, H_2, and of the $N_2 + 2H_2$ mixture, and on the background gas invasion into the pure jets. Besides the intrinsic and technological interest of this gas system, detailed in paper I, this study is intended to amend partially the scarcity of experimental data on shock waves of gas mixtures with large mass disparity, providing useful material to validate numerical procedures and theoretical models.[26]

The present work rests upon Raman spectroscopy diagnostics, which provides accurate data of number density and rotational temperatures of molecular gases, over a wide dynamic range. Such quantities are probed along and across the jet with a high spatial resolution and good sensitivity without disturbing the flow. This methodology has proved successful for the quantitative study of different phenomena in supersonic expansions of molecular gases,[27–32] including shock waves in pure jets.[11,12]

The paper is organized as follows. We briefly describe the main aspects of the experimental setup and the methodology as applied to N_2 - H_2 shock waves. Then we show the results from the measurements of normal and barrel shock waves in the pure gas jets, and those of the $N_2 + 2H_2$ mixture jet. Next, we discuss the Knudsen number in the pure N_2 shock waves, the species separation in the mixture, and the background gas

* To whom correspondence should be addressed: E-mail: angel.ramosgallardo@ciemat.es.

† Present address: Laboratorio Nacional de Fusión (CIEMAT), Avda. Complutense 22, E-28040 Madrid, Spain.

10.1021/jp1040053
Published on Web 07/01/2010

invasion through the shock wave system. We finish with a summary of the results and with some concluding remarks.

Experimental Section

The experimental setup and methodology have been described in detail in paper I, and only their more relevant aspects will be given here.

The shock waves were formed in continuous axisymmetric jets of N_2, H_2, and of $N_2 + 2H_2$, at stagnation pressure $p_0 = 1$ bar and temperature $T_0 = 295$ K, against a background pressure $p_b = 6.1 \pm 0.1$ mbar. The background pressure was measured with a MKS Baratron pressure gauge located 20 cm off-axis from the jet, at a point of negligible interaction with its wake. In these conditions the background gas is believed to be spatially uniform. The uncertainty of p_b was attributed to the instability of the pumping speed of the vacuum system. The gas samples were expanded through a cylindrical nozzle of diameter $D = 310\ \mu$m and internal length $L \approx 1.8$ mm, into a vacuum chamber devised for Raman spectroscopy measurements.

The $N_2 + 2H_2$ mixture was prepared in the feed line from the pure gases, each flowing through a Bronkhorst High-Tech mass flow controller with an accuracy of 0.9 mmol/min, up to reaching a stagnation pressure of 1 bar in the mixture. The nitrogen mole fraction $X_0(N_2)$ of a static sample of the so prepared mixture was measured by means of Raman spectroscopy in order to verify the molecular ratio, obtaining $X_0(N_2) = 0.34 \pm 0.01$.

A cw-Ar^+ laser ($\sim$4 W) was employed as excitation source at $\lambda = 514.5$ nm, the scattered Raman radiation being collected at 90° with respect to the laser beam and to the jet axis. The Raman spectra were recorded at $\sim$0.3 cm^{-1} spectral resolution.

The excitation-collection optical system was kept fixed along the experiment, and the nozzle was positioned to reach the point of interest in the flow field, with pointing accuracy of about $\pm 5\ \mu$m. Relative positions between two points are repeatable to $\pm 1\ \mu$m, which is the precision of the nozzle micropositioning actuators. The representative spatial resolution was about $0.05D$ ($\approx 15\ \mu$m) along and across the expansion axis; along the laser beam it ranges from $0.22D$ close to the nozzle, up to $1.2D$ in the farthest points.

The N_2 and H_2 number density n in a tiny volume of the expanding gas was obtained by measuring the Raman intensity scattered by that region (see paper I for details). For systematic plus random errors the total uncertainty (2σ = two standard deviations) of n is estimated in 5−10%.

The rotational temperature T_R was determined from the Raman intensities of rotational lines,[11,33,34] which are related to the populations P_J of the rotational levels J (see paper I for details). Outside the shock waves, the measured populations P_J of each nuclear spin species within the ground vibrational state very nearly obey a Boltzmann distribution, by means of which T_R is determined. The standard deviation due to random errors in the N_2 rotational temperatures is $\sim$1%; for *para*-H_2 (pH_2) it ranges from 1 to 3 K, and for *ortho*-H_2 (oH_2) from 1.5 to 5 K, depending on number density. These T_R values are nearly free from systematic errors.

Inside the shock waves the populations P_J depart markedly from a single Boltzmann distribution.[11] Therefore, in this region an alternative definition of rotational temperature has been used for N_2:

$$\langle T_R \rangle = \beta \sum_J P_J E_J \qquad (1)$$

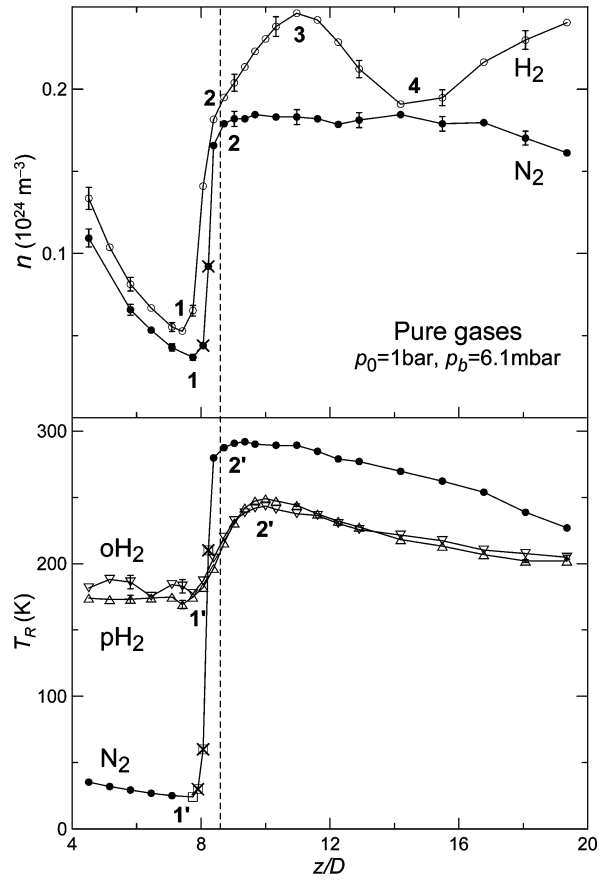

Figure 1. Number density n (top) and rotational temperature T_R (bottom) along the axis of the pure H_2 and N_2 jets across the normal shock wave. The vertical dashed line indicates the position of the shock wave according to eq 2. Open squares in N_2 temperatures indicate $\langle T_R \rangle$ according to eq 1. Cross symbols show the points in N_2 shock wave where Kn > 0.05. Representative $\pm\ \sigma$ error bars are shown.

where $\beta = hc/k = 1.4388$ cm K, and E_J is the energy in cm^{-1} of the rotational level J. The temperature $\langle T_R \rangle$ represents the average rotational energy per molecule expressed in Kelvin. Above the characteristic rotational temperature of the gas, under equilibrium conditions, $\langle T_R \rangle$ is equivalent to the temperature derived from a Boltzmann distribution.

The Raman spectra of N_2 recorded inside the present shock waves, and the corresponding Boltzmann plots showing the departure from a single Boltzmann distribution, are similar to those reported in Figure 4 of ref 11. In the spectra of H_2 the departure from Boltzmann distribution was not observed due to the very few rotational levels populated for each spin species at the temperatures of the experiments.

Results

Normal Shock Waves. Number density and rotational temperature were measured across the normal shock wave in the pure gas jets and in the $N_2 + 2H_2$ mixture. According to the expression[35,36]

$$z_M/D = 0.67\sqrt{p_0/p_b} \qquad (2)$$

the point of minimum impact pressure upstream from the normal shock wave for $p_0 = 1$ bar and $p_b = 6.1$ mbar is $z_M/D \approx 8.6$. The number densities n and the rotational temperatures T_R along the axis of the N_2 and H_2 jets are shown in Figure 1, where the

characteristic points 1, 2, 3, and 4 of normal shock waves[12] are indicated: points 1 and 1′ stand for the onset of n and T_R shock wave profiles, respectively; points 2 and 2′ mark the end of such profiles. The actual shock wave is encompassed between points 1 and 2 for n, and between 1′ and 2′ for T_R. It is well established that the thermal shock wave begins upstream from the density one,[11] that is, point 1′ should be closer to the nozzle than point 1; however, with the relatively coarse data sampling employed here the density and the thermal shock waves seem to start concurrently for each species. Point 3 is the first compression maximum after the shock wave, and point 4 indicates the minimum density in a secondary expansion in the wake.[37] Points 3 and 4 are particularly evident in the H_2 jet, whereas for N_2 they appear far downstream, outside the distance range studied here.[11,12]

The minimum density prior to the N_2 shock wave, point 1, is located at $z/D \approx 7.7$, about 10% closer to the nozzle than the position predicted by eq 2. At this point the Mach number is $M_1 = 7.9$ according to Miller's parametrization,[1] taking $M = 1$ at $z/D = -0.4$ as discussed in paper I. Considering these values and $\gamma = 7/5$, the Rankine−Hugoniot relation for the density ratio across the shock wave, $n_2/n_1 = 2.4M_1^2/(2 + 0.4M_1^2)$, yields $n_2 = 5.55\ n_1$ just after the shock wave. This n_2 value is ≈10% greater than the experimental density of N_2 at point 2. Such a deviation is not meaningful considering that Rankine−Hugoniot relations hold strictly for monodimensional shock waves of ideal gases, whereas the present jet is bidimensional[12] and the expanded gas is not ideal. The wake after the N_2 density jump (see Figure 1, top) is nearly a plateau with no significant feature, consistently with that of the shock wave located at $z/D \approx 9$ of a previous experimental study on N_2.[11,12]

The H_2 density profile shows marked differences with respect to that of N_2. The axial density in the zone of silence is greater than in the N_2 case, in agreement with the measurements of paper I, with point 1 located slightly upstream from that of N_2. Point 2 in the H_2 profile (see Figure 1, top) marks a discontinuity in the density slope, which is followed by an oscillatory pattern in the wake (points 3 and 4). This feature has been observed before in N_2 shock waves with higher Mach number, $M_1 > 10$, at $z_M/D > 15$.[11,12] The shock wave thickness, defined as $\delta = (n_2 - n_1)/\max(\mathrm{d}n/\mathrm{d}z)$, is $\delta \approx 120\ \mu$m for N_2, and $\delta \approx 220\ \mu$m for H_2, the difference being in qualitative correlation with the bulk viscosity $\eta_v\ (N_2) \ll \eta_v\ (H_2)$ and with the rotational collision number $Z\ (N_2) \ll Z\ (H_2)$.[38,39]

It is common practice in the literature to normalize the width of the normal shock density profile with the mean free path λ_1 at its onset. For this purpose, we employed the temperature-dependent mean free path[4]

$$\lambda(T) = [\sqrt{2}\pi d_{ref}^2 n (T_{ref}/T)^{\omega-1/2}]^{-1} \quad (3)$$

where d_{ref} is the variable soft sphere (VSS) molecular diameter at the reference temperature T_{ref}, and ω its viscosity index. For N_2, $d_{ref} = 4.11$ Å at $T_{ref} = 273$ K, and $\omega = 0.74$, yielding for the present pure N_2 jet $\lambda_1 \simeq 18\ \mu$m. With this λ, the normalized density profile is similar to that of shock wave "A" in Figure 6 of ref 11. In addition, its inverse shock thickness is $\lambda_1/\delta = 0.15$, about one-half of the value reported by Alsmeyer[8] for a one-dimensional N_2 shock wave for the same $M = 8$. However, this comparison must be taken with caution since the present flow is two-dimensional and the number of data points inside the shock wave is small.

The rotational temperature profile (Figure 1, bottom) shows a similar trend for both gases, but with quantitative differences due to their disparate rotational cross sections, as discussed in paper I. Within the shock wave, between points 1′ and 2′, the rotational populations of N_2 depart sharply from a single Boltzmann distribution,[11] so T_R between these points is estimated using eq 1, and is marked in Figure 1 with open square symbols. According to a previous interpretation,[11] such distribution of rotational population can be decomposed into two nearly-Boltzmann distributions, like in monatomic gas shock waves.[3] One set is formed by cold molecules coming from the zone of silence, and the other one by hot molecules that have collided in the shock wave. Once the rotational equilibrium is recovered, N_2 reaches a maximum $T_R \approx 292$ K (point 2′). At this point the estimated pressure $p = nkT$ (assuming $T = T_R$) is ≈7.3 mbar, which is higher than the background pressure $p_b = 6.1$ mbar. This may lead to a secondary expansion with associated cooling beyond point 2′, as shown in Figure 1, bottom. Hydrogen T_R shows a similar trend though with a far milder gradient across the normal shock wave than N_2, increasing from ≈180 K (point 1′) up to ≈250 K at point 2′; downstream from point 2′ it decreases in a similar way as in the N_2 jet. From point 1′ on, the two H_2 species, ortho and para, are in equilibrium with each other.

On the basis of the master equation that describes the evolution of rotational populations[40] the qualitative evolution across the normal shock wave of the translational T_T and the rotational T_R temperatures can be interpreted as follows. Upstream from point 1′, $T_R > T_T$, which is a necessary condition for the rotational cooling in the zone of silence. At point 1′ the crossing $T_R = T_T$ occurs, and between points 1′ and 2′ the condition $T_R < T_T$ holds, causing a rotational heating. Moreover, between these points a sharp maximum of T_T occurs, known as translational temperature overshoot,[5] corresponding to a minimum flow velocity in the shock wave. After this overshoot, T_T decreases crossing T_R again at point 2′. Downstream from point 2′, $T_R > T_T$, and so a secondary rotational cooling appears in the wake.

The thermal profile of H_2 is broader than in N_2, reaching its maximum temperature ≈1D downstream from the N_2 maximum (see Figure 1, bottom). The increase of T_R for H_2 is slower than that of N_2 and does not reach a maximum as high as in N_2 due to the very different rotational collision numbers $Z(N_2) \ll Z(H_2)$. Furthermore, the energy balance suggests flow velocity differences between N_2 and H_2 in the wake. The flow kinetic energy of the gas in a point is given by the difference between the gas energy at the source, related to T_0, and the total thermal energy in the point. In this way, at points 2′, where $T_R = T_T$, H_2 molecules have certainly more kinetic energy, and so a greater flow velocity, than the N_2 ones.

The normal shock wave in the jet of the $N_2 + 2H_2$ mixture is shown in Figure 2. Two features that are characteristic of monodimensional shock waves in binary mixtures of monatomic gases are observed. First, point 1 of the light component is located upstream from the corresponding point 1 of the heavy component.[16,21,22] Second, the temperature of the heavy component increases more steeply and exceeds that of the light one, reaching a sharp maximum inside the thermal shock wave profile of the light one.[41]

As shown in Figure 2, top, the density starts rising at $z/D \approx 7$ for H_2 and at $z/D \approx 8$ for N_2, resulting an inertial separation of the two both gases. Such effect produces an enrichment of the light species throughout most of the shock wave as discussed below. Between points 1 and 2, the thickness of the total density shock wave, $n(N_2) + n(H_2)$, is comparable to that of the pure H_2 jet (see Figure 1, top). Downstream from point 2 the density

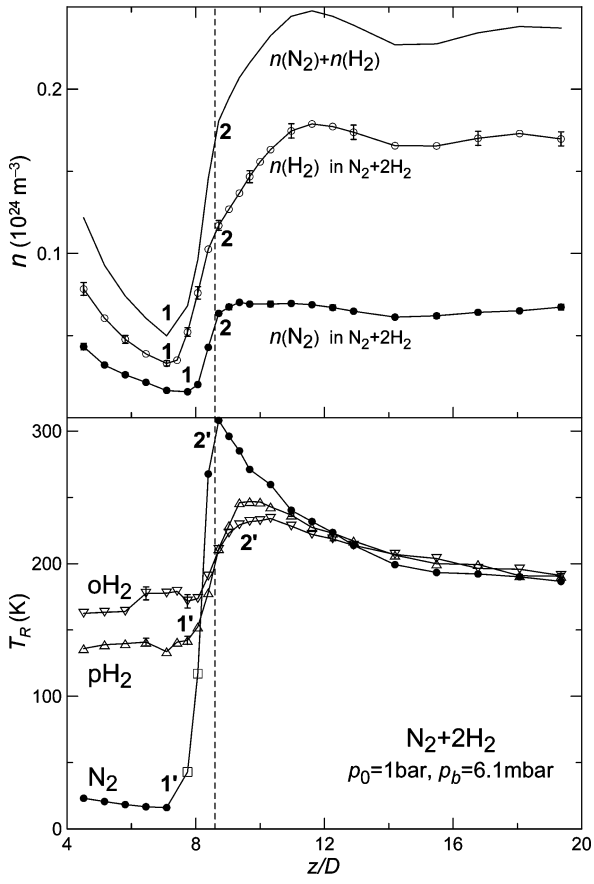

Figure 2. Number density n (top) and rotational temperature T_R (bottom) along the axis of the jet of the $N_2 + 2H_2$ mixture across the normal shock wave. The vertical dashed line indicates the position of the shock wave according to eq 2. Open squares in N_2 temperatures indicate $\langle T_R \rangle$ according to eq 1. Representative $\pm \sigma$ error bars are shown.

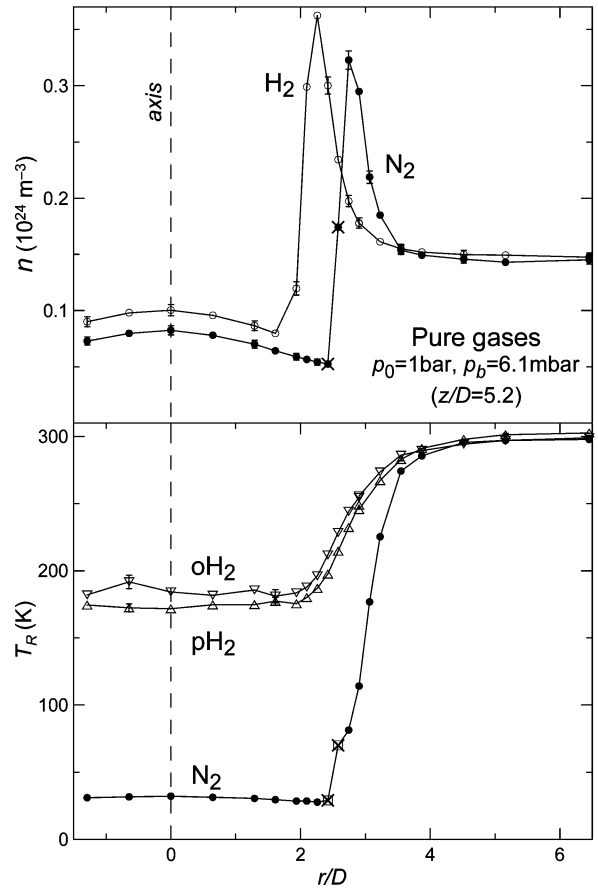

Figure 3. Number density n (top) and rotational temperature T_R (bottom) along the radial direction r at $z/D = 5.2$ of pure H_2 and N_2 jets. Open squares in N_2 temperatures indicate $\langle T_R \rangle$ according to eq 1. Cross symbols show the points where Kn > 0.05 in the N_2 jet. Representative $\pm \sigma$ error bars are shown.

profiles of the component gases in the mixture show the same features as in the pure jets, with an almost constant $n(N_2)$ along the wake, whereas $n(H_2)$ shows a change in its gradient and an oscillatory pattern, although less pronounced than in the pure jet (compare with Figure 1, top).

In the $N_2 + 2H_2$ mixture the rotational temperature of N_2 displays a sharp overshoot (point 2′) close to the end of the shock wave. Nitrogen T_R reaches a maximum of 308(2) K, 5% higher than the stagnation temperature T_0. Such an overshoot in monatomic mixtures has been reported to be more pronounced for hard shock waves and for large fraction of the light component.[17] Actually, a rotational temperature overshoot up to 12% of T_0 was observed in a shock wave of $N_2 + 4H_2$ mixture at $z/D \approx 6$.[24] Furthermore, the N_2 rotational overshoot occurs at a point where the H_2 temperatures are still increasing, reaching downstream a maximum of ≈240 K, well below T_0. This suggests an energy transfer from the light to the heavy component, consistent with $\sigma(N_2{:}H_2)$ (excitation/deexcitation of N_2 by H_2) being the largest inelastic rotational cross section, as concluded in paper I. Finally, a different evolution of the *ortho*- and *para*-H_2 species is observed in the mixture, with the T_R (pH_2) increasing in the shock wave above that of oH_2, as opposed to the pure jet, where the two species are nearly in equilibrium with each other (see Figure 1, bottom). At $z/D >$ 12 all the T_R of N_2 and H_2 are in equilibrium, decreasing slowly and monotonically.

Barrel Shock Waves. The n and T_R profiles of the pure H_2 and N_2 jets along a radial direction r perpendicular to the axis at $z/D = 5.2$ are shown in Figure 3. A sharp peak of the barrel shock waves appears clearly in the density profile of both jets, with the H_2 barrel shock broader and located closer to the axis than that of N_2. In consequence, the zone of silence of the H_2 jet is narrower than that of N_2 for the same p_0/p_b ratio. This is related to the Reynolds number at the source, $Re_0 \approx 3800$ for H_2 and 7000 for N_2, since the smaller Re_0, the narrower the zone of silence and the less definite the density barrel shock wave.[35]

In the zone of silence ($r/D < 2.5$) of the pure N_2 jet, the T_T calculated assuming an isentropic behavior departs from the experimental T_R by less than 5%. On the contrary, the T_R values of both H_2 species are well above their T_T values, as discussed in paper I. As shown in Figure 3, bottom, in the barrel shock waves T_R increases monotonically for *ortho*- and *para*-H_2, while for N_2 it shows up a step-like change in the profile at $r/D \approx$ 2.7, which is the position where the density is close to its maximum. In the first part of the N_2 temperature raise (points marked by open square symbols), up to the change in the slope, the rotational population P_J shows a non-Boltzmann distribution, as in the normal shock wave.

It should be noted that the maximum density in the barrel shock wave occurs in both pure N_2 and H_2 jets at the region where T_R starts increasing, and that n and T_R reach the background values at about the same point ($r/D \approx 4$). In addition, the pressure estimated as $p = nkT$ in the N_2 barrel shock, assuming $T = T_T = T_R$, increases monotonically up to the background pressure.

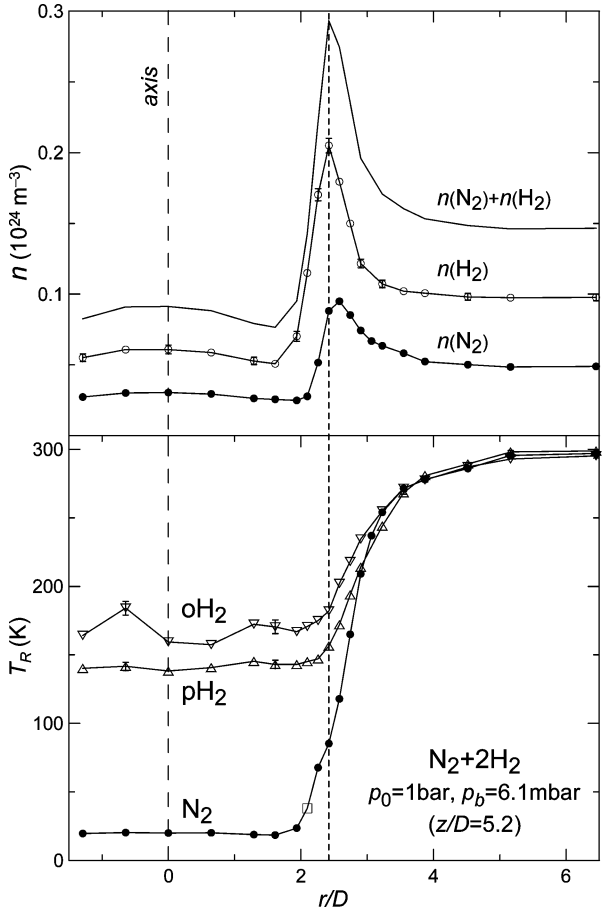

Figure 4. Number density n (top) and rotational temperature T_R (bottom) along the radial direction r at $z/D = 5.2$ of the $N_2 + 2H_2$ jet. Open squares in N_2 temperatures indicate $\langle T_R \rangle$ according to eq 1. The vertical dashed line at $r/D \approx 2.3$ is a visual guide, positioned at the maximum density point. Representative $\pm \sigma$ error bars are shown.

Number densities and T_R values for the jet of the $N_2 + 2H_2$ mixture along the radial direction r at $z/D = 5.2$ are shown in Figure 4. The total number density profile, $n(N_2) + n(H_2)$, shows a sharp maximum located at an intermediate position between those of the pure H_2 and N_2 jets shown in Figure 3. The separate density profiles of the two gases in the mixture show slightly broader peaks than in the jets of the pure gases, lying very close to each other, with N_2 maximum about 10% closer to the jet axis than in the pure N_2 jet. Outside the barrel shock wave of the mixture, the decrease of the n (N_2) and n (H_2) profiles toward the background density is somewhat slower than in the pure jets; this behavior is more evident for n (N_2). The difference between these profiles causes the enrichment of the heavy species immediately outside the barrel maximum, as discussed below.

The rotational temperatures of both gases in the mixture follow the same radial trend as in the pure jets, although with some differences worth to be mentioned. In the zone of silence, for $r/D \leq 2$, the T_R values in the mixture are lower than in the pure jets, with a larger gap between *ortho*- and *para*-H_2, in agreement with previous measurements of paper I. In the mixture, $T_R(H_2)$ begins to rise after density increases, like in the pure H_2 jet. On the contrary, $T_R(N_2)$ in the mixture starts to rise prior to density and closer to the axis than in the pure N_2 jet; actually, $T_R(N_2)$ in the mixture seems to follow the total number density profile, $n(N_2) + n(H_2)$, with a smooth step-like feature at the point of the total density maximum. As for the pure jet, at the beginning of the temperature rise the N_2 rotational

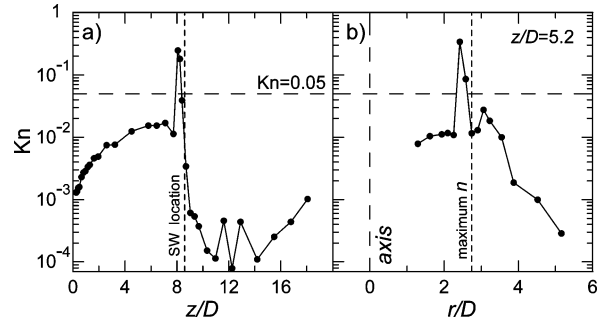

Figure 5. Knudsen number, eq 4 and 5, for the pure N_2 jet, (a) along the jet axis, taking $l = z$; and (b) along the radial direction, $l = r$, at $z/D = 5.2$. The vertical dashed line in (a) indicates the position of the normal shock wave according to eq 2.

populations are out of equilibrium, with a non-Boltzmann distribution (open square symbol in Figure 4, bottom). Outside the barrel shock wave, the two gases in the mixture are in thermal equilibrium for $r/D \geq 3.5$.

Knudsen Number. A parameter of interest in the analysis of supersonic flows is the local Knudsen number

$$\mathrm{Kn} = \lambda / L \tag{4}$$

where λ is the mean free path, and

$$L = \frac{q}{\mathrm{d}q/\mathrm{d}l} \tag{5}$$

is the scale length of the macroscopic gradient of the quantity q.[4] At low Kn the gas can be described as a continuum, an approach that fails at high Kn, like in highly rarefied flows or in shock waves. The upper limit $\mathrm{Kn} = 0.05$ has been proposed[42] for the continuum equations to be valid, whereas for higher Kn the flow has to be described with discrete particle models.

The local Kn for the number density of the pure N_2 jet across its normal and barrel shock waves, estimated from the measured n and with λ calculated according to eq 3, is shown in Figure 5. It should be noted that on the jet axis the density gradient vector points along the axis itself, while at the barrel shock wave such gradient vector is slightly off the radial direction r; this adds some degree of uncertainty to the estimated Kn along r. For most of the flow field Kn is less than 0.02. In the zone of silence Kn increases as the gas rarefies with the expansion until the onset of the shock waves, where Kn suddenly peaks to values above 0.05. The maxima of Knudsen number are ≈0.25 in the normal shock wave and ≈0.34 in the barrel shock wave.

In the N_2 shock waves the points where $Kn > 0.05$ are indicated in Figure 1 and Figure 3 by cross symbols. The rotational populations P_J at these points depart markedly from a Boltzmann distribution. According to its definition (eq 4 and 5), Kn is a ratio between the mean free path and the distance along which the flow quantity q changes by a significant amount. Large Kn means that molecules travel between consecutive collisions through a region with significantly different flow properties, either because of lack of collisions (highly rarefied flows) or very large gradients (shock waves). In either case, under these circumstances it is difficult for the gas to maintain the equilibrium in this region. As a result, different sets of molecules coexist within the shock wave, with different velocity and population distributions, and so the whole cannot be described by a single Boltzmann distribution.[2] The invasion of

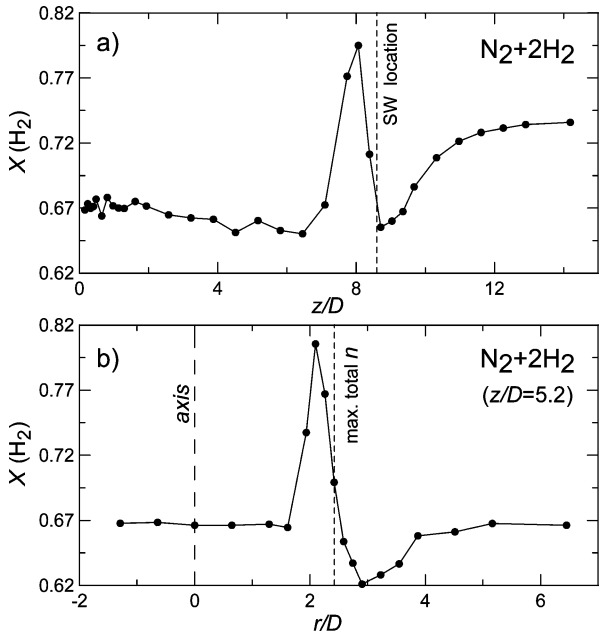

Figure 6. Hydrogen mole fraction $X(H_2)$ in the jet of the $N_2 + 2H_2$ mixture, (a) along the jet axis across the normal shock wave, and (b) along the radial direction at $z/D = 5.2$, crossing the barrel shock wave. The vertical dashed line in (a) indicates the position of the normal shock wave according to eq 2.

background gas across shock waves is also conditioned by Kn, as discussed below.

Species Separation. In paper I we reported on the species separation in the zone of silence of $N_2 + 2H_2$ and $2N_2 + H_2$ jets, with the normal shock wave located at $z/D \approx 30$, far away from the nozzle. These results were compared with Sherman's theory of diffusive separation.[43] Here we discuss a different enrichment effect, under the same source conditions but different background pressure. This effect, which was not considered by Sherman's theory, turns to be associated to shock waves.

The mole fraction $X(H_2)$ measured along the jet axis of the $N_2 + 2H_2$ mixture is shown in Figure 6a. At $z/D \approx 6$, not far from the normal shock wave, a shallow minimum of $X(H_2) \approx 0.65$ is observed, which corresponds to $X(N_2) = 1 - X(H_2) \approx 0.35$, providing a mild enrichment of ≈6% for the heavier species with respect to the first axial data. Comparing this enrichment with that reported in paper I for the same gas mixture, significant differences are observed. While in the present jet $X(N_2)$ shows no substantial variation up to $z/D \approx 2$, in paper I most of the enrichment occurs for $z/D < 2$. Moreover, the highest enrichment of N_2 observed here is significantly less than the value ∼12% obtained in paper I. These differences can be attributed to the proximity of the shock wave structure, which disturbs the diffusive separation in the zone of silence.

The shallow minimum of $X(H_2)$ is followed by a sharp maximum $X(H_2) \approx 0.8$ located at $z/D \approx 8$, immediately upstream from the predicted position of the normal shock wave, implying a highly localized enrichment of ≈20% of the light species. This is due to the delay of the heavy species density profile in the normal shock wave, as shown in Figure 2, top. Downstream from the shock wave, $X(H_2)$ steeply drops to the minimum values found in the zone of silence. Then a slow increase along the wake follows, which is attributed to the preferential penetration of background H_2 as discussed below.

The $X(H_2)$ profile across the barrel shock wave at $z/D = 5.2$ is shown in Figure 6b. A sharp increment of $X(H_2)$ up to ∼20% of its source value is observed in the internal side of the barrel shock. A depletion of H_2 is observed in the external side, followed by a slow increase of $X(H_2)$ with radial distance up to the background value at $r/D \approx 4$. These strong variations of $X(H_2)$ are due to the different positions and widths of the density peaks of both gases in the barrel shock wave, shown in Figure 4.

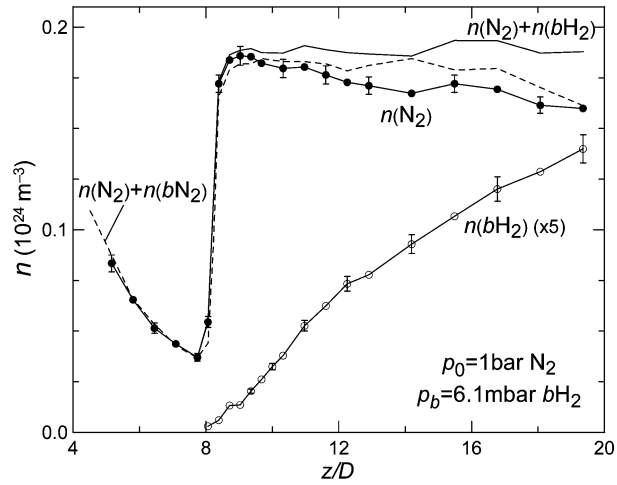

Figure 7. Number density along the axis of the pure N_2 jet against background hydrogen (bH_2) across the normal shock wave; $n(bH_2)$ is magnified ×5. The dashed line depicts the number density of the pure N_2 jet shown in Figure 1. Representative ± σ error bars are shown.

This species separation observed in the shock waves can be explained in terms of an inertial effect, since the heavier molecules have more momentum than the lighter ones for the same velocity. In the normal shock wave the strong deceleration leads to the delayed rise of the density profile of the heavy species with respect to the light one. In the barrel shock wave, the change of flow direction deflects heavier molecules to a lesser extent and leads to a significant enrichment of the lighter species in the internal side of the barrel shock wave, as seen in the present results. Furthermore, this last separation can be reinforced by diffusive effects like those described in the next section. Such an inertial separation is the basis of the aerodynamic focusing effect,[44] which has been applied to species separation, from isotopes to aerosols, mostly by means of converging nozzles or obstacles driving the flow. To our knowledge, such a high enrichment of the lighter species in the barrel shock wave has not been reported previously. Combining this effect with a suited system of concentric skimmers might provide the basis for a highly efficient species separation device.

Invasion of the Jet by the Background Gas. The invasion of the jet by background molecules through the shock wave system was studied here in two jets, one of pure N_2 against background H_2, and another of pure H_2 against background N_2. The background pressures were maintained fixed at 6.1 mbar, as for the shock waves shown above.

The penetration of background H_2 into the wake and normal shock wave of the pure N_2 jet is shown in Figure 7. Far downstream from the shock wave the background H_2 molecules represent about a 15% of the total, decreasing with the distance to the normal shock wave. Some background H_2 does cross the N_2 normal shock wave, reaching the beginning of the N_2 density raise, where H_2 amounts to ∼1% of the total molecules. Similar measurements in the jet of H_2 against background N_2 have shown that N_2 does not reach the axial region of the wake, and it is detected off-axis, just at $r/D > 1.5$. This preferential invasion of H_2 into the wake may explain the H_2 enrichment downstream from the normal shock wave of the $N_2 + 2H_2$ jet shown in Figure 6a.

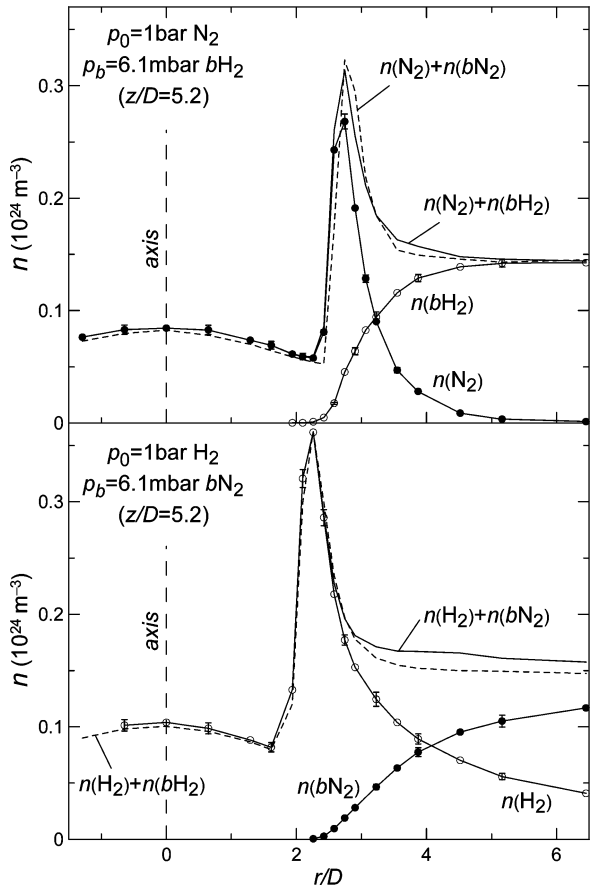

Figure 8. Number density across the barrel shock wave of (top) the pure N_2 jet against background hydrogen (bH_2), and (bottom) of the pure H_2 jet against background nitrogen (bN_2). The dashed lines depict the pure gas densities of Figure 3. Representative $\pm\,\sigma$ error bars are shown.

The number densities across the barrel shock wave at $z/D = 5.2$ of the N_2 jet against background H_2 are shown in Figure 8, top, and for the H_2 expanded against background N_2 in Figure 8, bottom. It can be seen that the total density, expanded plus background gas, in these jets agrees well with the independent data of the pure jets shown in Figure 3, although the N_2 and H_2 abundances differ markedly between both cases. Outside the barrel shock wave the density of the expanded gas decreases faster for N_2 than for H_2. In turn, H_2 penetrates deeper than N_2 into the barrel. Background H_2 was detected as close to the axis as $r/D \approx 2$, about at the edge of the zone of silence, representing $\sim$2% of the total molecules. On the contrary, the innermost point where background N_2 was detected ($\sim$ 0.2% of total molecules) was $r/D \approx 2.2$, about the point of maximum H_2 density. The present results on normal and barrel shock waves confirm the preferential invasion of the free jet by the lighter species of a background gas mixture reported elsewhere.[19]

Other experiments on the invasion of supersonic rarefied plasma jets by background gas[45,46] concluded that part of the molecules in the zone of silence come indeed from the background gas, crossing the barrel shock wave. Numerical simulations of those jets[47] yielded values of the local Knudsen number (eq 4) greater than 0.1 in an extensive region of the zone of silence. With such large Knudsen numbers it may be expected that a significant fraction of the molecules that cross the barrel shock could reach the jet axis. On the contrary, the present jets, with Kn < 0.02 in the zone of silence, are denser than those plasma jets, therefore the background molecules are not expected to penetrate deep into the zone of silence.

Summary and Conclusions

In this work we have shown the power of Raman spectroscopy for the quantitative study of shock waves displaying strong density and temperature gradients where two molecular species of large mass ratio are involved, namely N_2 and H_2. This study shows the complex features of normal and barrel shock waves associated with axisymmetric supersonic jets of a $N_2 + 2H_2$ mixture, employing the pure N_2 and H_2 jets as references.

A number of quantitative differences have been observed between N_2 and H_2 density and rotational temperature profiles of the shock waves in the mixture. In particular the lag between the density profiles of both species in the normal shock wave as well as in the barrel shock wave leads to a noticeable enrichment of the light species. This enrichment is far from monotonous, showing a highly localized peak close to the position of the shock wave density maximum. Clearly, it differs in nature from that observed at the beginning of the zone of silence of similar jets reported in paper I. It is tempting to speculate about the possibility of employing this enrichment at the barrel shock wave for practical purposes.

Marked differences of the rotational temperature profiles have been observed in the shock waves of the $N_2 + 2H_2$ mixture compared to those of the pure species. Such differences can be attributed to the contribution of the inelastic collisions between N_2 and H_2 in the mixture. The state-to-state cross sections of such collisions are expected to be larger than those of N_2:N_2 and H_2:H_2 collisions of the pure species, according to paper I. On the other hand, the shock wave profiles have been shown to strongly depend on the volume viscosity,[39] a quantity that rests entirely on the inelastic cross sections.[38] Thus, in the long term, a full characterization of the shock wave profiles, and of the concomitant enrichment process, at a molecular level will require a detailed knowledge of the inelastic collisions of the species in the mixture. Although the state-to-state cross sections for N_2:N_2 and H_2:H_2 collisions have already been studied at a preliminary level,[31,32] the corresponding quantities for N_2:H_2 collisions have not been approached yet, neither at theoretical nor at experimental level.

The permeability of the barrel and normal shock waves to the background gas has also been studied, observing a clear evidence of the preferential pass of the light species through the shock wave barrier boundaries. This provides additional support in favor of the species separation mechanism reported time ago.[19] The observed preferential pass of the light species through the shock wave depends in molecular terms on the N_2:N_2, H_2:H_2, N_2:H_2 and H_2:N_2 diffusion coefficients, which in turn depend also on the collision cross sections and are still poorly known, like the volume viscosity.

Although the items mentioned above are roughly known at a qualitative level by the specialized scientific community, the severe lack of experimental data on particular cases, and the still more severe lack on collision cross sections impede a firm progress toward the efficient characterization of many related problems of scientific and technical relevance. It is hoped that the overview reported in this paper, and the data provided in more detail as Supporting Information, will contribute to some extent to move in the direction of understanding the molecular mechanisms underlying shock waves in multispecies gases.

Acknowledgment. A. R. acknowledges CSIC for an I3P grant. This work has been supported by the Spanish Ministerio de Educación y Ciencia, research Projects Nos. FIS2004-02576 FIS2007-61430, CSD2009-0038 (ASTRO-MOL), and by the Comunidad de Madrid, Project No. S-0505/ESP/0237 (ASTRO-CAM).

Supporting Information Available: Supporting tables are available with the experimental data of the number densities and the rotational temperatures plotted in Figures 1−4, 7, and 8. This material is available free of charge via the Internet at http://pubs.acs.org.

References and Notes

(1) Miller, D. R. Free jet sources In *Atomic and Molecular Beam Methods*; Scoles, G., Ed.; Oxford University Press, 1988; Vol. I, Ch. 2.
(2) Mott-Smith, H. M. *Phys. Rev.* **1951**, *82*, 885–892.
(3) Pham-Van-Diep, G.; Erwin, D.; Muntz, E. P. *Science* **1989**, *245*, 624–626.
(4) Bird, G. A. *Molecular Gas Dynamics and the Direct Simulation of Gas Flows*; Clarendon Press: Oxford, 1994.
(5) Koura, K. *Phys. Fluids* **1997**, *9*, 3543–3549.
(6) Robben, F.; Talbot, L. *Phys. Fluids* **1966**, *9*, 633–643.
(7) Robben, F.; Talbot, L. *Phys. Fluids* **1966**, *9*, 653–662.
(8) Alsmeyer, H. *J. Fluid Mech.* **1976**, *74*, 497–513.
(9) Mazouffre, S.; Vankan, P.; Engeln, R.; Schram, D. C. *Phys. Rev. E* **2001**, *64*, 066405.
(10) Miles, R. B.; Lempert, W. R.; Forkey, J. N. *Meas. Sci. Technol.* **2001**, *12*, R33–R51.
(11) Ramos, A.; Maté, B.; Tejeda, G.; Fernández, J. M.; Montero, S. *Phys. Rev. E* **2000**, *62*, 4940–4945.
(12) Graur, I. A.; Elizarova, T. G.; Ramos, A.; Tejeda, G.; Fernández, J. M.; Montero, S. *J. Fluid Mech.* **2004**, *504*, 239–270.
(13) García-Colín, L. S.; Velasco, R. M.; Uribe, F. J. *Physics Reports* **2008**, *465*, 149–189.
(14) Riabov, V. V. *J. Thermophys. Heat Transfer* **2003**, *17*, 526–533.
(15) Maltsev, R. V.; Plotnikov, M. Y.; Rebrov, A. K. *Phys. Fluids* **2007**, *19*, 106102.
(16) Kosuge, S.; Aoki, K.; Takata, S. *Eur. J. Mech. B - Fluids* **2001**, *20*, 87–126.
(17) Raines, A. *Eur. J. Mech. B - Fluids* **2002**, *21*, 599–610.
(18) Park, C. *J. Thermophys. Heat Transfer* **1993**, *7*, 385–398.
(19) Campargue, R. *J. Chem. Phys.* **1970**, *52*, 1795–1802.
(20) Brook, J. W.; Calia, V. S.; Muntz, E. P.; Hamel, B. B.; Scott, P. B.; Deglow, T. L. *J. Energy* **1980**, *4*, 199–208.
(21) Rothe, D. E. *Phys. Fluids* **1966**, *9*, 1643–1658.
(22) Center, R. E. *Phys. Fluids* **1967**, *10*, 1777–1784.
(23) Harnett, L. N.; Muntz, E. P. *Phys. Fluids* **1972**, *15*, 565–572.
(24) Bochkarev, A. A.; Kosinov, V. A.; Prikhod'ko, V. G.; Rebrov, A. K. *J. Appl. Mech. Tech. Phys.* **1972**, *13*, 804–808.
(25) Ramos, A.; Tejeda, G.; Fernández, J. M.; Montero, S. *J. Phys. Chem. A* **2009**, *113*, 8506−8512.
(26) Boyd, I. D.; VanGilder, D. B.; Beiting, E. J. *AIAA J.* **1996**, *34*, 2320–2326.
(27) Montero, S.; Maté, B.; Tejeda, G.; Fernández, J. M.; Ramos, A. Raman studies of free jet expansions (diagnostics and mapping) In *Atomic and Molecular Beams. The State of the Art 2000*; Campargue, R., Ed.; Springer-Verlag: 2001.
(28) Maté, B.; Graur, I. A.; Elizarova, T. G.; Chirokov, I.; Tejeda, G.; Fernández, J. M.; Montero, S. *J. Fluid Mech.* **2001**, *426*, 177–197.
(29) Tejeda, G.; Fernández, J. M.; Montero, S.; Blume, D.; Toennies, J. P. *Phys. Rev. Lett.* **2004**, *92*, 223401.
(30) Ramos, A.; Fernández, J. M.; Tejeda, G.; Montero, S. *Phys. Rev. A* **2005**, *72*, 053204.
(31) Montero, S.; Thibault, F.; Tejeda, G.; Fernández, J. M. *J. Chem. Phys.* **2006**, *125*, 124301.
(32) Fonfría, P.; Ramos, A.; Thibault, F.; Tejeda, G.; Fernández, J. M.; Montero, S. *J. Chem. Phys.* **2007**, *127*, 134305.
(33) Tejeda, G.; Maté, B.; Fernández-Sánchez, J. M.; Montero, S. *Phys. Rev. Lett.* **1996**, *76*, 34–37.
(34) Maté, B.; Thibault, F.; Tejeda, G.; Fernández, J. M.; Montero, S. *J. Chem. Phys.* **2005**, *122*, 064313.
(35) Ashkenas, H.; Sherman, F. S. The structure and utilization of supersonic free jets in low density wind tunnels In *4th Rarefied Gas Dynamics*; de Leeuw, J. H., Ed.; Academic Press: New York, 1966; Vol. II, pp 84−105.
(36) Young, W. S. *Phys. Fluids* **1975**, *18*, 1421–1425.
(37) Panda, J.; Seasholtz, R. G. *Phys. Fluids* **1999**, *11*, 3761–3777.
(38) Zhdanov, V. M. *Transport Processes in Multicomponent Plasma*; Taylor & Francis: Bristol, USA, 2002.
(39) Elizarova, T. G.; Khokhlov, A. A.; Montero, S. *Phys. Fluids* **2007**, *19*, 068102.
(40) Ramos, A.; Tejeda, G.; Fernández, J. M.; Montero, S. *Phys. Rev. A* **2002**, *66*, 022702.
(41) Abe, K.; Oguchi, H. *Phys. Fluids* **1974**, *17*, 1333–1334.
(42) Boyd, I. D.; Chen, G.; Candler, G. V. *Phys. Fluids* **1995**, *7*, 210–219.
(43) Sherman, F. S. *Phys. Fluids* **1965**, *8*, 773–779.
(44) Fernández de la Mora, J.; Rosell-Llompart, J. *J. Chem. Phys.* **1989**, *91*, 2603–615.
(45) Engeln, R.; Mazouffre, S.; Vankan, P.; Schram, D. C.; Sadeghi, N. *Plasma Sources Sci. Technol.* **2001**, *10*, 595–605.
(46) Vankan, P.; Mazouffre, S.; Engeln, R.; Schram, D. C. *Phys. Plasmas* **2005**, *12*, 102303.
(47) Abbate, G.; Kleijn, C. R.; Thijsse, B. J.; Engeln, R.; van de Sanden, M. C. M.; Schram, D. C. *Phys. Rev. E* **2008**, *77*, 036703.

JP1040053